

Accepted Manuscript

Non destructive monitoring of cavitation erosion of cordierite based coatings

Marko Pavlović, Marina Dojčinović, Sanja Martinović, Milica Vlahović, Zoran Stević,
Tatjana Volkov Husović



PII: S1359-8368(16)30525-X

DOI: [10.1016/j.compositesb.2016.04.073](https://doi.org/10.1016/j.compositesb.2016.04.073)

Reference: JCOMB 4272

To appear in: *Composites Part B*

Received Date: 10 March 2016

Revised Date: 13 April 2016

Accepted Date: 24 April 2016

Please cite this article as: Pavlović M, Dojčinović M, Martinović S, Vlahović M, Stević Z, Volkov Husović T, Non destructive monitoring of cavitation erosion of cordierite based coatings, *Composites Part B* (2016), doi: 10.1016/j.compositesb.2016.04.073.

This is a PDF file of an unedited manuscript that has been accepted for publication. As a service to our customers we are providing this early version of the manuscript. The manuscript will undergo copyediting, typesetting, and review of the resulting proof before it is published in its final form. Please note that during the production process errors may be discovered which could affect the content, and all legal disclaimers that apply to the journal pertain.

Non destructive monitoring of cavitation erosion of cordierite based coatings

Marko Pavlović^a, Marina Dojčinović^a, Sanja Martinović^b, Milica Vlahović^{b*},

Zoran Stević^c, Tatjana Volkov Husović^a

^a*University of Belgrade, Faculty of Technology and Metallurgy, 4 Karnegijeva St.,
Belgrade, Serbia*

^b*University of Belgrade, Institute of Chemistry, Technology and Metallurgy, 12 Njegoševa
St., Belgrade, Serbia*

^c*University of Belgrade, Technical Faculty in Bor, 12 Vojske Jugoslavije St., Bor, Serbia*

* Corresponding author. Tel.: +381-11-3303-698; fax: +381-11-3370-389.

E-mail address: milica.vlahovic@yahoo.com (Milica Vlahović).

Abstract

Coating materials are widely used in refractory lining to prevent different deleterious effects such as reactions on the mold-metal contact surface, abrasion from liquid metal or alloy, gasses, slags, and other materials in contact with the coating. In this paper, behavior of cordierite based coating exposed to the cavitation erosion was investigated. Cordierite samples sintered at 1200 and 1400 °C were used for the tests. Mass loss, level of surface degradation obtained using image analysis and thermal imaging analysis were applied for the cavitation erosion evaluation. Results showed that the cordierite samples can be successfully used in conditions where the cavitation resistance is required.

Keywords: A. Ceramic-matrix composites (CMCs); B. Defects; D. Non-destructive testing; D. Surface analysis.

1. Introduction

An extremely lightweight material, cordierite ($2\text{MgO}-2\text{Al}_2\text{O}_3-5\text{SiO}_2$), with low thermal expansion and excellent strength, rigidity and thermal shock resistance is an excellent candidate for different industrial applications [1-5].

Cordierite is mainly a structural ceramic material, often used for kiln furniture due to its extremely good thermal shock resistance. Like other structural ceramic materials, it also has good thermal and electrical insulating capabilities. In engineering practice, mechanical properties of materials play a major role in determining their suitability for specific applications. These mechanical properties are related to the crystalline phase and microstructure of the materials. Desirable properties of ceramic systems can be obtained by the proper selection of the stoichiometric composition required for the formation of the

crystalline phases. Development of fine-grained microstructures in ceramics improves the thermo-mechanical properties [6]. The formation of ceramics is influenced by the composition, the choice of nucleating agents, and also by the performed treatment processes [7].

Cavitation involves the formation, growth, and collapse of bubbles in a liquid due to the local pressure changes. This phenomenon can occur if the pressure in a liquid is reduced sufficiently to cause formation of bubbles or vapor-filled voids. When a liquid is subsequently subjected to higher hydrostatic pressure, the bubbles can collapse and cause pressure waves and microjets. If these collapses are repeated, the solid surface in the liquid is subjected to the fatigue, which can cause the cavitation erosion. Cavitation erosion is a type of wear that occurs in many types of hydraulic structures such as pumps, valves, water turbines, ship propellers. Previous studies were occupied with the cavitation erosion of many kinds of materials: gray cast irons with graphite phase, stainless steels, coated materials and Ni–P–SiC composite coatings, and ceramic materials such as sialon, silicon carbide, and silicon nitride ceramics [8-18]. However, cavitation damage test is usually used for metallic materials. Recent studies are mainly based on designing and developing modern materials as well as replacing metallic components with composite and ceramic materials. Over the last few decades, considerable efforts have been devoted to enhancing the erosion resistances of different alloys and steel by deposition of protective coatings on their surfaces [9-14]. The coatings can be easily formed on the surface of steel, which can exhibit smooth surface and good mechanical properties; such are high hardness, high elastic modulus, and high oxidation resistance [13]. Many fluid machinery components are supplied with coatings to prolong their lifetime and to improve their work efficiency.

Nowadays, combined usage of modeling and nondestructive testing (NDT) is a consolidated practice in order to study the physical condition of a component, above all in the aeronautical and aerospace fields [19-22].

Image analysis of the sample surface degradation is an important non-destructive method for assessing damage of the materials. Namely, image analysis provides more objective characterization of materials from the aspect of their properties. Evaluation of various materials properties, as well as the effect of external influences on their microstructure, can be investigated using this methodology. The Image Pro Plus is a special program for processing and analysis of image [23].

Among the NDT techniques, the infrared thermography (IRT) is the only diagnostic technology allowing the operator to instantly visualize and verify the thermal material performance [24]. Active thermography represents a non-destructive technique (NDT) and it is based on observing the temperature differences with an infrared camera after a thermal excitation, and can be analyzed by various methods: lock-in thermography (LT), pulse thermography (PT), and pulsed phase thermography (PPT) [25].

In order to estimate level of subsurface anomalies quantitatively, it is necessary to apply advanced algorithms to the raw curves [26,27]; in this way, it is possible to gather information, such as depth and dimensions of the subsurface anomalies [27,28] and also, in some cases, their nature [29,30].

In this study attention was focused on investigating the cavitation erosion resistance of the cordierite samples sintered at different temperatures. Accordingly, the idea was to investigate behavior and possible application of cordierite coatings under extreme conditions of the cavitation exposure. Level of cavitation damage was monitored by mass

loss and surface erosion of the tested material. Coupling between properties and structure of the samples sintered at two different temperatures as well as their influence on damage level caused by cavitation was the main task of this study. The obtained results can be used for finding other possible applications of cordierite coatings.

2. Experimental

2.1 Materials

Cordierite ($2\text{MgO}\cdot 2\text{Al}_2\text{O}_3\cdot 5\text{SiO}_2$) as refractory coating is selected in accordance with the following properties: high refractoriness (16 SK/1470°C), hardness by Mosh scale 7, density 1.9-2.2 g/cm³; low coefficient of thermal conductivity ($\lambda= 2.3\text{-}2.9$ W/mK); low coefficient of linear thermal expansion ($\alpha=1.7\cdot 10^{-6}$ °C⁻¹ (20-1000°C)); high resistance to thermal shock; relatively high melting temperature with the possibility of application to 1380 °C; high inertness to the liquid metal (does not develop fumes in contact with liquid metal); low wettability with the liquid metal.

Cordierite used for the samples preparation was synthesized using the following materials: kaolin, alumina, and sepiolite, whose chemical composition is given in Table 1. The initial materials except kaolin, which was in powder form, were crushed to the upper limit of size 100 % $-0.1\cdot 10^{-3}$ m. Then, the components were mixed according to the following amounts: 35 mass% of alumina (maximum particle size of 0.1 mm), 28 mass% of sepiolite (maximum particle size of 0.1 mm), and 37 mass% of kaolin (< 63 μm). After homogenization, the mixture powder was pressed under the pressure of 1 MPa and sintered

at the temperature of 1200 and 1400 °C for 2 hours in the laboratory furnace with an oxidation atmosphere.

Composition of the synthesized cordierite samples is as follows: 51.11 % SiO₂, 30.9 % Al₂O₃, 13.5 % MgO, 1.29 % Fe₂O₃, and 3.2 % CaO.

In order to determine size and shape factor of particles, which is important for preparation of coating materials, the obtained material was mechanically activated for 60 min in vibratory mill with the upper limit of size 100 % -40·10⁻⁶ m to a grain size of 100 % -24·10⁻⁶ m.

Size and shape factor of particles were measured using 3510 and 3240 grains, respectively. Average particle size was 24.45 μm (100 % -24 x 10⁻⁶ m). Minimum and maximum measured grain sizes were 4.88 and 86.30 μm, respectively. The standard deviation was $\sigma = 16.44$. Middle shape factor was 0.67. Based on this data, the grain of the sample belongs to the category of rounded grains. Maximum and minimum shape factors were 0.85 and 0.29, respectively. The standard deviation was $\sigma = 0.15$.

Particle size distribution and grain shape factors of the sample before sintering are shown in histograms presented in Figures 1 and 2.

Figure 1.

Figure 2.

XRD of sintered cordierite samples is given in Figure 3.

Figure 3.

In the Figure 3 a), the sample sintered at 1200 °C exhibits typical pattern of cordierite with the following phases: cordierite, cristobalite, spinel, ortopyroxen, forsterite, garnet and silimanit. Diffraction pattern of cordierite sintered at 1400 °C, given in Figure 3 b), shows the dominant presence of cordierite rich with iron and minor amount of ringwoodite.

SEM analysis of cordierite samples sintered at 1200 and 1400 °C is given in Figure 4.

Figure 4.

As can be seen, morphology of the samples is similar. The sample sintered at 1200 °C shows parts with the porosity (dark part at the surface). For the sample sintered at 1400 °C, the amount of pores is lower and their surface areas are smaller.

2.2 Methods

2.2.1 Cavitation erosion testing

Cavitation erosion testing was performed according to the procedure described by ASTM G32 standard. The ultrasonic vibratory cavitation set up and stationary specimen method were applied. The set up consisted of: a high frequency generator of 360 W, an electro-strictive transducer, a transformer for mechanical vibrations, and a water bath containing the test specimen. Cavitation erosion testing was accomplished by utilizing the

recommended standard values: mechanical vibration frequency (20 ± 0.2 kHz); mechanical vibrations amplitude at the top of the transformer (50 ± 2 μm); gap between the test specimen and the transformer (0.5 mm); water bath temperature (25 ± 1 °C); ordinary water flow (5-10 ml/s).

The same conditions developed for metallic materials testing were applied to the cordierite samples. These parameters were controlled throughout the testing process.

The cavitation damage level was determined by monitoring the mass loss and the surface degradation during the experiment. Total duration of the cavitation tests was 80 min.

Mass loss of the test specimens was measured by analytical balance with an accuracy of ± 0.1 mg. Before being weighted, the test specimens were dried at 110 °C until the constant mass. The measurements were performed after each 10 min of subjecting the test specimens to the cavitation.

Surface degradation was monitored by image analysis of sample surface photographs using Image Pro Plus program as well as thermographic images [8-10,15,31-33].

In order to provide reliability of obtained results, cavitation experiments were done using three samples of both series for each testing period. Accordingly, the presented results of mass loss and surface degradation are average values of three measurements.

2.2.2 Image analysis

Image analysis was added to the standard laboratory procedure of measuring the mass loss with the aim to monitor surface erosion caused by the cavitation and to determine

level of surface damage. Photographs of the sample surfaces were analyzed by Image Pro Plus, special software program that enables work in all known formats of images (TIFF, JPEG, BMP, TGA). It automatically measures, counts and classifies data on analyzed objects. Program communicates directly with Excel, thus enabling statistical and graphical treatment of data. Results were presented as the surface degradation level (P/P_0) during the testing time. Since certain degradation was noticed at the sample surface even before the tests, P_0 was determined according to the ideal facets (surface area without any defects). P was measured surface area destructed during the testing. Based on the correlation of these results with the material properties, behavior of the investigated material can be analyzed [8-10,15].

2.2.3 *ThV testing*

To perform presented testing experiments, two IR lamps of 250W were used as thermal excitation source. IR camera FLIR E60 with the spectral range from 7.5 to 13 μm , thermal sensitivity of 50 mK at 30 $^{\circ}\text{C}$, MSX 320 x 240 resolution, and frame rate of 60 Hz was used. In the post-processing of thermogram sequences after step of heating, FLIR Tools + software was used to determine the temperature profiles and histograms.

3. Results and Discussion

3.1 Mass change

Mass loss results of sintered cordierite samples during the cavitation erosion testing are given in the Figure 5.

Figure 5.

According to the obtained results presented at the Figure 5, the mass loss was higher for the cordierite samples sintered at 1200 °C compared to the samples sintered at 1400 °C. The difference between mass losses of the samples is increasing with the duration of testing time. Samples sintered at 1400 °C exhibited more stable behavior during the experiment, as mass loss was 8.63 mg after 60 minutes and for the samples sintered at 1200 °C mass loss was 39.01 mg, for the same time. It is obvious that sintering temperature has significant influence on the cavitation erosion resistance of the cordierite samples.

3.2 Image analysis

Photographs of sintered cordierite samples before and during the cavitation erosion testing are given in Figure 6.

Figure 6.

According to the photographs presented in Figure 6, the surface area of the samples sintered at 1200 °C is covered with small pits whose number is increasing during the testing. However, cordierite samples sintered at 1400 °C showed different surface damage, as larger pits are forming during the testing compared with the samples sintered at 1200 °C. These results correspond to the results of the surface degradation level given in Figure 7.

Figure 7.

As shown in Figure 7, during the entire testing period, cordierite samples sintered at 1200 °C exhibited higher surface degradation level than the samples sintered at 1400 °C. These results are in accordance with the mentioned increasing number of small pits during the testing of the samples sintered at 1200 °C. Oppositely, for the samples sintered at 1400 °C, the main mechanism is related to the formation of larger pits from the beginning of the testing and to their growth during the testing. This claim can be supported by SEM microphotographs of typical pits at the end of the testing period for both cordierite samples, Figure 8.

Figure 8.

It is obvious that for the samples sintered at 1200 °C, pit areas are smaller and their depths are also smaller (Figure 8 a)), compared to the samples sintered at 1400 °C (Figure 8 b)).

Besides, Image Pro Plus offers line profile for further analysis of surface degradation level. The appropriate color channel was chosen and applied on the images of the sintered cordierite samples at the end of the cavitation testing while RGB mode was selected. Based on the analysis of the samples images using red, blue or green color channel, the best resolution between damaged and undamaged surfaces was obtained using blue color channel. After choosing filter channel, line profile option by sample diameter was applied. Figure 9 represents photographs of sintered cordierite samples at the end of cavitation testing as well as the obtained line profiles.

Figure 9.

Considering the cordierite samples sintered at 1200 °C (Figure 9 a)), degraded surface area is obvious and visible, as part of the line profile in the center of the sample exhibits maximum differences in intensity, thus indicating large amount of small pits. For the cordierite samples sintered at 1400 °C (Figure 9 b)), maximum differences in intensity of the whole line profile are much greater, which indicates larger pits compared with the sample sintered at 1200 °C. This observation corresponds with the previously given surface degradation level. The above approach can be useful as an additional analysis of the surface degradation for the purpose of estimating amount and size of existing pits.

3.3 Thermal imaging

Cordierite samples after 80 minutes of cavitation erosion testing were heated by two IR lamps for 90 seconds and then cooled for 630 seconds. Thermal changes at their surfaces, which provide to discover zone with defects, can be noticed after only 15 seconds of cooling.

Cooling curves for cordierite samples sintered at different temperatures after cavitation testing and IR- heating, presenting changes of the maximum temperature with cooling time in defect zone, are given in the Figure 10.

Figure 10.

Cooling curves indicate lower density of the sample sintered at 1200 °C (Figure 10 a)) compared with the sample sintered at 1400 °C (Figure 10 b)), which is in agreement with the fact that the density of materials rises with increasing the sintering temperature. Based on the initial parts of the curves, where the temperature changes are larger, time for post-processing analysis (line temperature profiles and temperature distribution histograms) was determined and then adequate thermograms were chosen.

For this analysis, thermograms of the samples sintered at 1200 °C and 1400 °C after cooling time of 390 seconds were chosen and presented in Figure 11 a), c) and Figure 12 a), c), respectively. Another reason for choosing these conditions is clear representation of the damaged and undamaged zones of the samples. Figure 11 b), d) and Figure 12 b), d) show line temperature profiles and temperature distribution histograms of cordierite samples sintered at 1200 °C and 1400 °C, after 390 seconds of cooling, respectively.

Figure 11.

Figure 12.

Based on the obtained results for thermal imaging, some differences in behavior of samples sintered at various temperatures can be observed.

The thermograms given in Figure 11 a), c) and Figure 12 a), c) represent differences in damaged and undamaged zones, which correlate with the photographs in Figure 8. Based on the temperature line profiles, shown in Figure 11c) and Figure 12c), damaged and undamaged zones cannot be distinguished precisely. These results can be useful only for

distribution of the defects. The temperature distribution histograms, presented in Figure 11d) and Figure 12d), indicate more regular temperature distribution of the cordierite samples sintered at 1200 °C compared to those sintered at 1400 °C. Also, according to the temperature distribution histograms, pits depths of cordierite samples sintered at 1200 °C in deformation zone are approximately the same, while cordierite samples sintered at 1400 °C exhibit greater differences in their pits depths. This correlates with the results obtained by image analysis.

Thermography offers noncontact, wide area for detection of subsurface defects, and can be used as an alternative or complement method to the conventional inspection technologies [24,25]. To improve detection of the deformation, it is necessary to apply a IR camera with higher graphical and thermal resolution [27]. The introduction of lock-in system would also be a great improvement [29].

4. Conclusion

Behavior of the cordierite samples sintered at different temperatures (1200 and 1400 °C) and subjected to the cavitation erosion testing was monitored using mass loss, image analysis for determination of surface degradation level and line profile, as well as thermal imaging for obtaining temperature line profiles and temperature distribution histograms.

Obtained results pointed out the following conclusions:

- Samples sintered at various temperatures showed different defect formation mechanisms, as well as level and distribution of the surface defects;
- Samples sintered at 1200 °C are characterized by large number of small pits whose number is increasing with the time of cavitation exposure;

- Samples sintered at 1400 °C are characterized by forming larger pits but in lower amount compared to the samples sintered at 1200 °C;
- The image analysis results, expressed through the surface degradation level and line profile, can be correlated to the size and number of pits formed during the cavitation;
- Thermal analysis indicated that the most useful results can be obtained from the temperature distribution histograms, which are in accordance with the image analysis results;
- Cordierite samples can be used for application in conditions where cavitation erosion resistance is needed.

Acknowledgments

This research has been financed by Ministry of Education, Science and Technological Development of the Republic of Serbia as part of the projects TR 33007, III 45012, TR 35002 and ON 172060.

References

- [1] Awano M, Takagi H. Synthesis of cordierite and cordierite-ZrSiO₄ composite by colloidal processing. *J Mater Sci* 1994;29:412–8.
- [2] Hirano M, Inada H. Preparation and characterization of cordierite-zirconia composites from co-precipitated powder. *J Mater Sci* 1993;28:74–8.
- [3] Sun EH, Chooa Y-H, Sekino T, Niihara K. Fabrication and mechanical properties of cordierite/ZrO₂ composites by pressureless sintering. *J Ceram Process Res* 2000;1(1):9–11.

- [4] Yamuna A, Johnson R, Mahajan YR, Lalithambika M. Kaolin-based cordierite for pollution control. *J Eur Ceram Soc* 2004;24:65–73.
- [5] Tang B, Fang YW, Zhang SR, Ning HY, Jing CY. Preparation and characterization of cordierite powders by water-based sol–gel method. *Indian J Eng Mater Sci* 2011;18:221–6.
- [6] Marikkannan SK, Ayyasamy EP. Synthesis, characterisation and sintering behaviour influencing the mechanical, thermal and physical properties of cordierite-doped TiO₂. *J Mater Res Technol* 2013;2:269-75.
- [7] Shamsudin Z, Hodzic A, Soutis C, Hand RJ, Hayes SA, Bond IP. Characterization of thermo-mechanical properties of MgO-Al₂O₃-SiO₂ glass ceramic with different heat treatment temperatures. *J Mater Sci* 2011;46:5822–9.
- [8] Pędzich Z, Jasionowski R, Ziąbka M. Cavitation wear of structural oxide ceramics and selected composite materials. *J Eur Ceram Soc* 2014;(34):3351-6.
- [9] Martinovic S, Dojcinovic M, Dimitrijevic M, Devecerski A, Matovic B, Volkov Husovic T. Impementation of image analysis on thermal shock and cavitation resistance testing of refractory concrete. *J Eur Ceram Soc* 2010;30:3303–9.
- [10] Martinovic S, Vlahovic M, Dojcinovic M, Volkov-Husovic T, Majstorovic J. Thermomechanical properties and cavitation resistance of a high-alumina low cement castable. *Int J Appl Ceram Tec* 2011;8(5):1115–24.
- [11] Hammitt FG. Cavitation and multiphase flow phenomena. New York: McGraw-Hill, 1980.
- [12] Knapp RT, Daily JW, Hammitt FG. Cavitation. New York: McGraw-Hill, 1970.
- [13] Okada T, Iwai Y, Hattori S, Tanimura N. Relation between impact load and the damage produced by cavitation bubble collapse. *Wear* 1995;184:231-9.

- [14] Hattori S, Mori H, Okada T. Quantitative evaluation of cavitation erosion. *J Fluid Eng-T ASME* 1998;120 (1):179-85.
- [15] Dojcinovic M, Volkov-Husovic T. Cavitation damage of the medium carbon steel: Implementation of image analysis. *Mater Lett* 2008;62:953-6.
- [16] Gong X, He W, Li Z, Gui L, Han J, Liu Q, Meng J, Lu J. Microstructural effect of α -Sialon ceramic on the resistance to cavitation erosion in deionized water. *Ceram Int* 2014;40(5):7161-69.
- [17] Chen X, Yan J, Ren S, Wang Q, Wei J, Fan G. Microstructure, mechanical properties, and bonding mechanism of ultrasonic-assisted brazed joints of SiC ceramics with ZnAlMg filler metals in air. *Ceram Int* 2014;40(1)(Part A):683-9.
- [18] Zhou X, Lin B, Yan S, Wang A, Zhang X, Ge S. Influence of temperature and concentration on tribological properties of silicon nitride in glycerol aqueous solution. *Ceram Int* 2016;42(3):3786-96.
- [19] Toscano C, Meola C, Carlomagno GM. Porosity distribution in composite structures with infrared thermography. *J Comp* 2013;2013:1-8.
- [20] Zhou D, Tian GY, Li Y. Simulation based on optimization of pulsed eddy current probe design. *NDT&E* 2010;25(3):219-30.
- [21] Markov AA, Mosyagin VV, Keskinov MV. A program for 3D simulation of signals for ultrasonic testing of specimens. *Russ J Nondestruct+* 2005;41(12):778-89.
- [22] Yamawaki H, Moriya S, Masuoka T, Takatsubo J. Computer simulation of ultrasonic testing for aerospace vehicle. *J Phys Conf Ser* 2011;278:1-4.

- [23] Vlahović M, Savić M, Martinović S, Boljanac T, Volkov-Husović T. Use of image analysis for durability testing of sulfur concrete and Portland cement concrete. *Mater Design* 2012;34:346-54.
- [24] Maldague XPV. *Theory and practice of infrared technology for nondestructive testing*. New York:John Wiley & Sons, 2001.
- [25] Carosena M. A new approach for estimation of defects detection with infrared thermography. *Mater Lett* 2007;(61)(3):747-50.
- [26] Sfarra S, Ibarra-Castanedo C, Santulli C, Sarasini F, Ambrosini D, Paoletti D, Maldague XPV. Eco-friendly laminates: from the indentation to non-destructive evaluation by optical and infrared monitoring techniques. *Strain* 2013;(49)(2):175-89.
- [27] Sfarra S, Ibarra-Castanedo C, Ambrosini D, Paoletti D, Bendada A, Maldague X. Integrated approach between pulsed thermography, near-infrared reflectography and sandwich holography for wooden panel paintings advanced monitoring. *Russ J Nondestruct+* 2011;(47)(4):284-93.
- [28] Crinière A, Dumoulin J, Ibarra-Castanedo C, Maldague X. Inverse model for defect characterization of externally glued CFRP on reinforced concrete structures: Comparative study of square pulsed and pulsed thermography. *Quant Infrared Thermogr J* 2014;(11)(1):84-114.
- [29] Duan Y, Huebner S, Hassler U, Osman A, Ibarra-Castanedo C, Maldague XPV. Quantitative evaluation of optical lock-in and pulsed thermography for aluminum foam material. *Infrared Phys Tech* 2013;(60):275-80.

- [30] Theodorakeas P, Ibarra-Castanedo C, Sfarra S, Avdelidis NP, Kouli M, Maldague XPV, Paoletti D, Ambrosini D. NDT inspection of plastered mosaics by means of transient thermography and holographic interferometry. *NDT & E Int* 2012;(47):150-6.
- [31] Sfarra S, Ibarra-Castanedo C, Ridolfi S, Cerichelli G, Ambrosini D, Paoletti D, Maldague X. Holographic interferometry (HI), infrared vision and X-ray fluorescence (XRF) spectroscopy for the assessment of painted wooden statues: a new integrated approach. *Appl Phys A-Mater* 2014;115(3):1041-56.
- [32] Martinovic S, Vlahovic M, Boljanac T, Dojcinovic M, Volkov Husovic T. Cavitation resistance of refractory concrete: Influence of sintering temperature. *J Eur Ceram Soc* 2013;33(1):7-14.
- [33] Vlahović M, Jovanić P, Martinović S, Boljanac T, Volkov-Husović T. Quantitative evaluation of sulfur-polymer matrix composite quality, *Compos Part B: Eng* 2013;44(1):458-66.

Figure captions

Figure 1. Histogram of particle size distribution of the sample before sintering

Figure 2. Histogram of grain shape factors of the sample before sintering

Figure 3. XRD of cordierite samples sintered at a) 1200 °C and b) 1400 °C

Figure 4. SEM microphotographs of cordierite samples sintered at: a) 1200 °C and b) 1400 °C

Figure 5. Mass loss of sintered cordierite samples during the cavitation erosion testing

Figure 6. Photographs of sintered cordierite samples before and during cavitation erosion testing

Figure 7. Surface degradation level of sintered cordierite samples before and during cavitation erosion testing

Figure 8. SEM microphotographs of cordierite samples sintered at a) 1200 °C and b) 1400 °C, after cavitation testing

Figure 9. Photographs of cordierite samples sintered at a) 1200°C and b) 1400°C after implementation of blue filter and corresponding line profiles

Figure 10. Cooling curve (maximum temperature versus time) for cordierite samples sintered at a) 1200 °C, and b) 1400 °C.

Figure 11. Cordierite sample sintered at 1200 °C after 390 s of cooling: a, c)

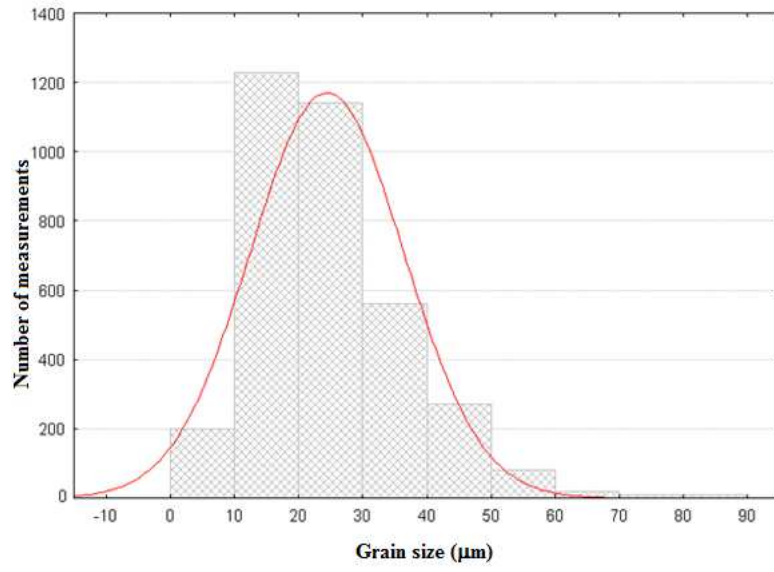
Thermographic images; b) Temperature line profile; d) Temperature distribution histogram

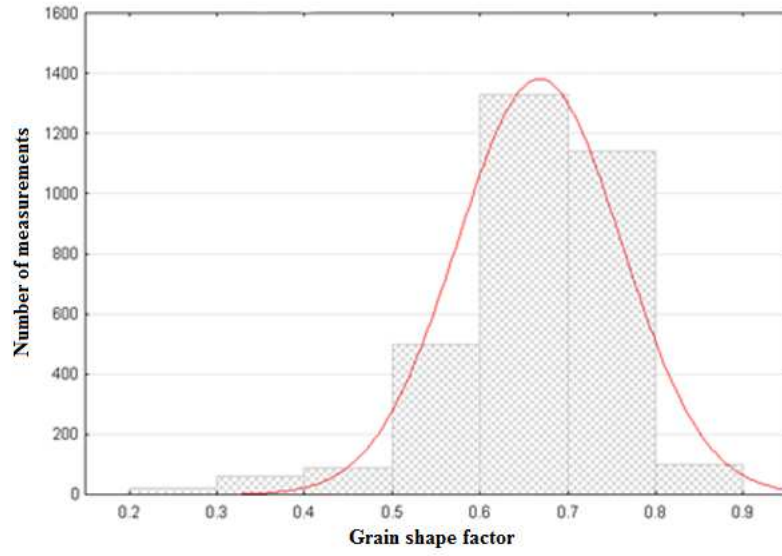
Figure 12. Cordierite sample sintered at 1400 °C after 390 s of cooling: a, c)

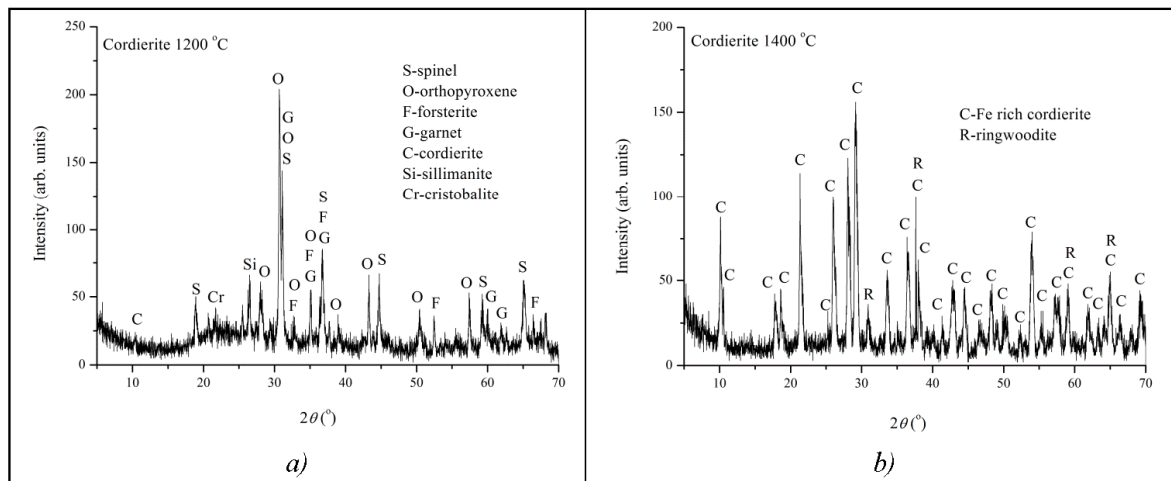
Thermographic images; b) Temperature line profile; d) Temperature distribution histogram

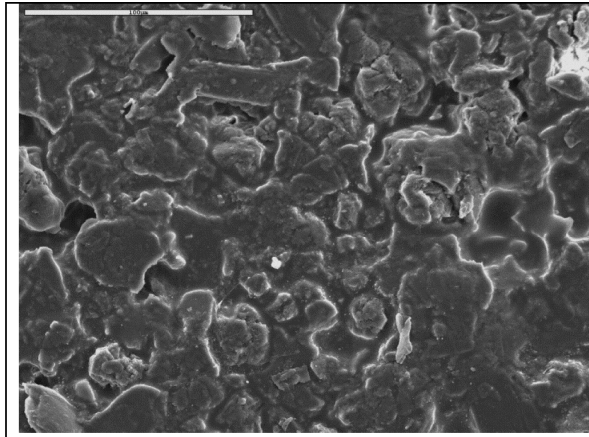
Tables*Table 1. Composition of starting components for cordierite synthesis*

Composition (%)							
Precursor	SiO ₂	MgO	Al ₂ O ₃	Fe ₂ O ₃	CaO (%)	Na ₂ O+K ₂ O	LOI
Alumina	0.14	0.01	95.96	0.09	0.16	0.05	3.20
Sepiolite	52.33	29.25	1.19	0.22	0.54	0.18	18.50
Kaolin	53.55	/	28.93	1.35	0.65	0.07	8.14

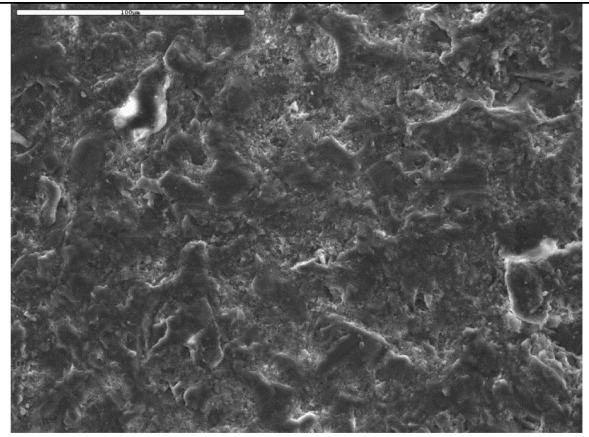






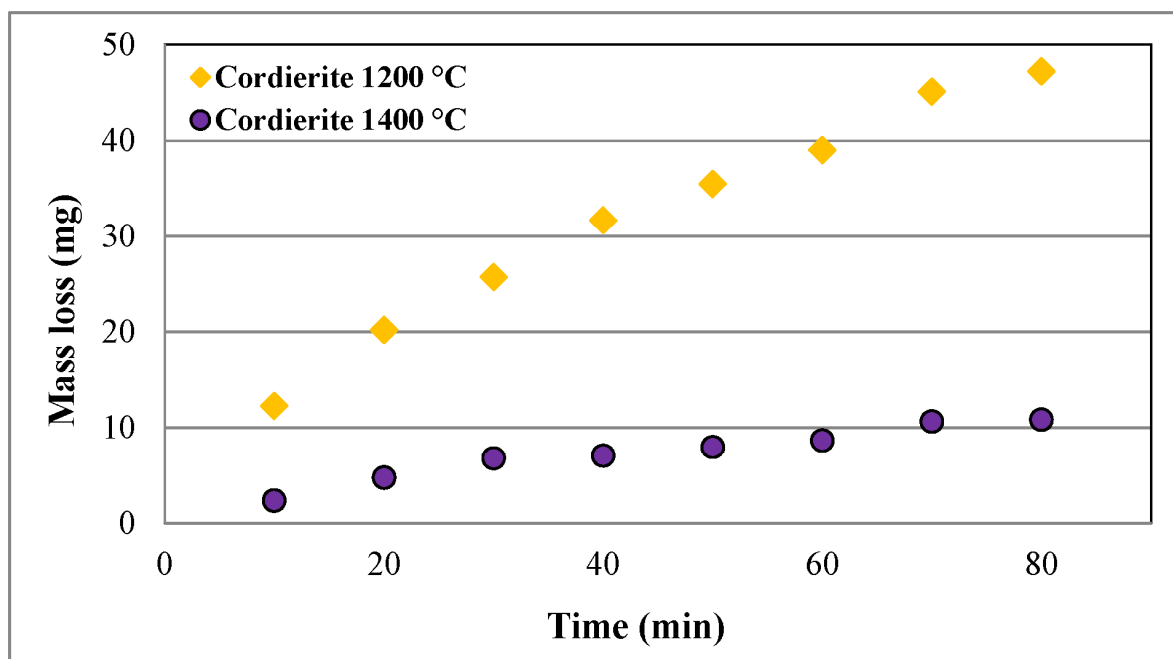









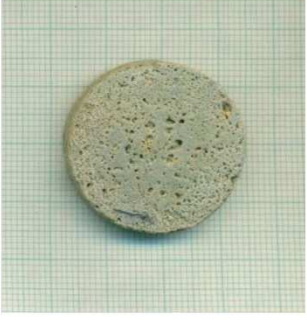


a)



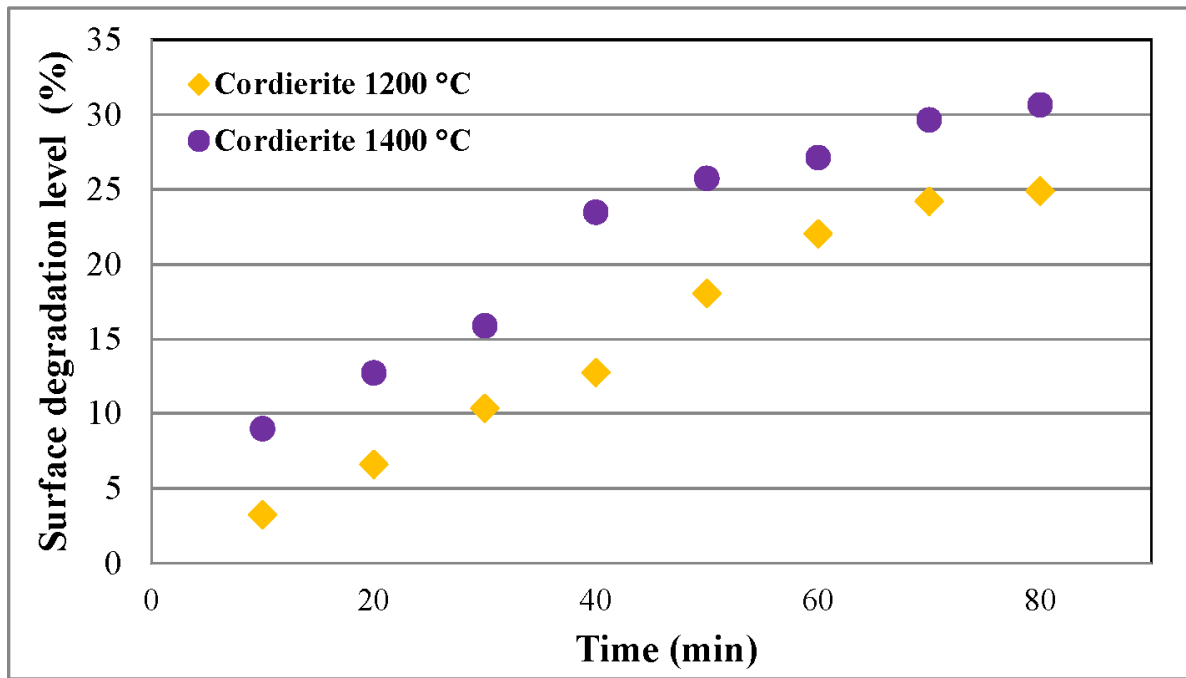
b)

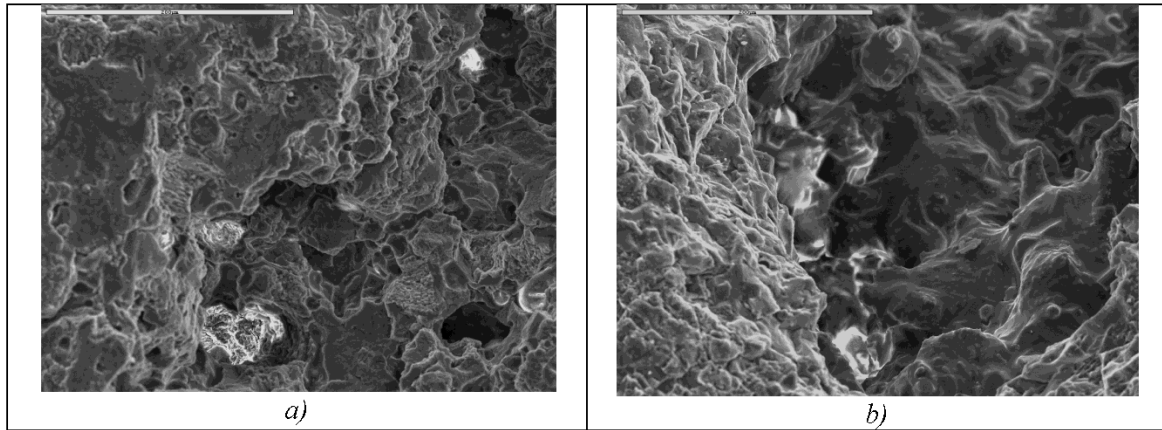
ACCEPTED MANUSCRIPT



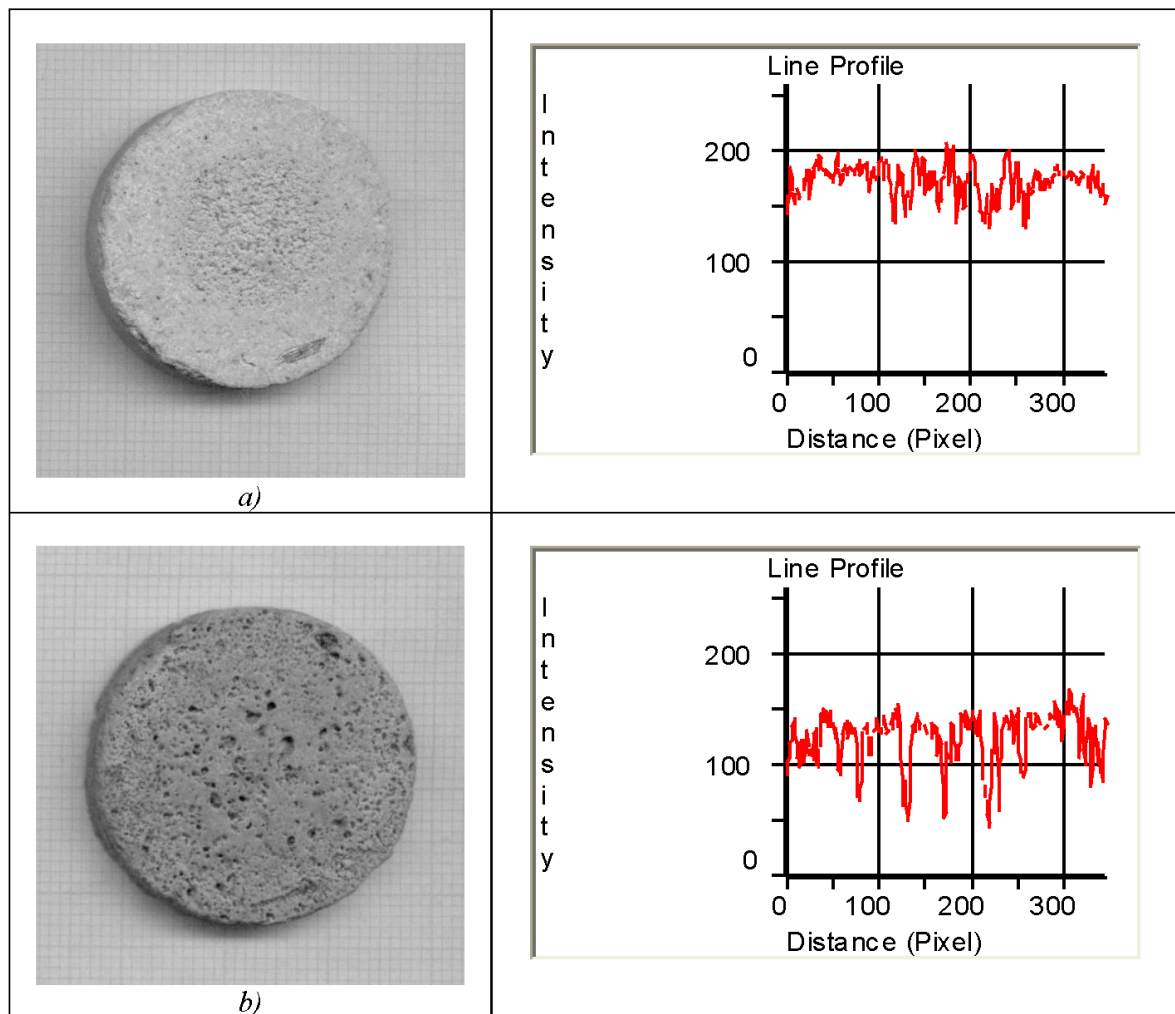
Time (min)	1200 °C	1400 °C
0		
20		
40		
60		
80		

ACCEPT

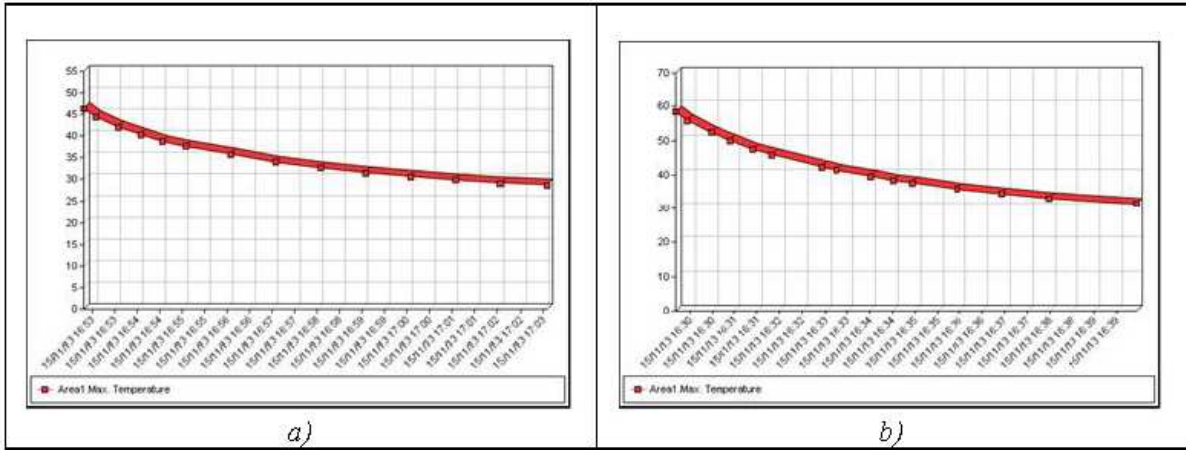




ACCEPTED MANUSCRIPT



ACCEPTED



ACCEPTED MANUSCRIPT

